Adsorption (2007) 13: 21–32
DOI 10.1007/s10450-007-9006-8

Simplified gauge-cell method and its application to the study of capillary phase transition of propane in carbon nanotubes

José P.B. Mota · Isabel A.A.C. Esteves

Received: 23 June 2006 / Revised: 31 October 2006 / Accepted: 3 January 2007 / Published online: 7 April 2007

Abstract A modification of the gauge-cell method for Monte Carlo studies of phase equilibrium in nano-confined systems is presented and employed for studying the capillary phase transition of propane in single-walled carbon nanotubes as a function of tube diameter. It is shown that if an analytical equation of state for the vapor phase is known, the acceptance rule for the trial move of particle exchange can be modified to reference the bulk system through its chemical potential. Under these conditions, the simulation procedure is simplified and acquires many characteristics of a Monte Carlo simulation conducted in the grand canonical ensemble. It is also shown that the critical temperature can be estimated by interpolation of sub- and supercritical values of the slope of the inverse isotherm at the inflection point. To enhance the sampling of propane molecules in the hollow space of the nanotubes the configurational-bias scheme is employed. The simulation results show that the confinement of propane increases its critical density, reduces the critical temperature and narrows the binodal curve with decreasing tube diameter until the system approaches one-dimensional behavior.

Keywords Gauge-cell method · Molecular simulation · Single-walled carbon nanotubes · Capillary phase transition · Propane adsorption

1 Introduction

Single-walled carbon nanotubes (SWNTs) are receiving increasing interest due to their remarkable physicochemical and electronic properties (Baughman et al. 2002). The hollow nanoscaled structure of SWNTs is especially attractive for their use as membranes (Hinds et al. 2004), hydrogen storage media for fuel cell technology (Darkrim et al. 2002), removal of hazardous pollutants from gaseous streams (Long and Yang 2001), adsorbents, catalyst supports and related materials (Harrys 1999). These applications may be realized by availability of more detailed information on the porosity and adsorption mechanisms of these materials.

A large number of experimental studies have already been carried out on the adsorption of small molecules (Kuznetsova et al. 2000; Muris et al. 2000; Yoo et al. 2002a, 2002b; Cinke et al. 2003) and larger organic vapors (Hilding et al. 2001; Agnihotri et al. 2005b) on various carbon nanotubes, single- or multiwalled, closed- or open-ended. Molecular simulations have also been performed to study gas adsorption on carbon nanotubes (Simonyan et al. 1999; Yin et al. 1999; Williams and Ecklund 2000; Duren and Keil 2001; Calbi et al. 2001; Talapatra and Migone 2002; Levesque et al. 2002; Ohba and Kaneko 2002; Zhang and Wang 2002; Shi and Johnson 2003; Jiang and Sandler 2003; Agnihotri et al. 2005a; Jiang et al. 2005), but very few have addressed phase transitions inside nanotubes (Peterson et al. 1990; Maddox and Gubbins 1995; Jiang et al. 2004). This is unfortunate because fluids confined in nanotubes may exhibit a variety of states, such as layer transitions, freezing transitions, and capillary transitions (Evans 1990; Gelb et al. 1999), and computer simulation methods are particularly useful for their study (Heffelfinger et al. 1987, 1988; Gelb and Gubbins 1997a, 1997b; Zhang and Chakrabarti 1994).

The grand canonical ensemble provides a natural framework for studying adsorption in porous materials since it is representative of a system at fixed chemical potential. The corresponding Monte Carlo simulation (GCMC) allows to

J.P.B. Mota (✉) · I.A.A.C. Esteves
Requimte/CQFB, Departamento de Química, Faculdade de Ciências e Tecnologia, Universidade Nova de Lisboa, 2829-516 Caparica, Portugal
e-mail: pmota@dq.fct.unl.pt

obtain adsorption isotherms of fluids in any pore geometry and to locate the equilibrium phase transition from the equality of the grand thermodynamical potential. The latter is computationally expensive because the grand thermodynamical potential must be obtained by thermodynamic integration (Peterson and Gubbins 1987; Peterson et al. 1988). GCMC simulations may also be used to locate a phase transition by histogram-reweighting (Alvarez et al. 1999; Shi et al. 2002).

A direct approach for simulating the coexistence curve of a confined fluid is the pore–pore Gibbs ensemble Monte Carlo (GEMC) method (Panagiotopoulos 1987a), but its applicability is restricted to pore geometries that allow continuous variation of the simulation cell volume, while preserving periodic boundary conditions. The pore–pore GEMC method gives directly the densities of the coexisting phases in a single-component system. However, the method does not yield the equilibrium chemical potential at which phase coexistence occurs. This can be circumvented by estimating the chemical potential from the trial step of particle exchange (Frenkel and Smit 1996), which is equivalent to the Widom test particle method (Widom 1963).

Since the pore–pore GEMC method only provides subcritical data, the usual approach to estimate the critical properties is by extrapolation from weighted linear fits of the subcritical simulation data to scaling laws for the order parameter $(\rho_L - \rho_V)/2\rho_c$ and diameter $(\rho_L - \rho_V)/2$ (Rowlinson and Widom 1982). This should be done with care (Panagiotopoulos 1994), however, since the accuracy of the coexistence data deteriorates in the immediate vicinity of the critical point. This is because close to the critical point the fluids in the two simulation cells may exchange their identities and densities are subjected to large fluctuations. The pore–pore GEMC method has been extensively employed in studies of capillary condensation and liquid–liquid equilibria (Panagiotopoulos 1987a; McGrother and Gubbins 1999; Vishnyakov and Neimark 2001; Lastoskie et al. 1993; Gozdz et al. 1995; Vishnyakov et al. 2001; Brovchenko et al. 2001, 2004a; 2004b).

Recently, Neimark and Vishnyakov (Neimark and Vishnyakov 2000; Vishnyakov and Neimark 2001) proposed the gauge-cell Monte Carlo simulation method, which is superior to the GCMC method for the simulation of the complete adsorption isotherm, including the stable, metastable, and unstable regions. The method is in essence a restricted version of the GEMC method (Panagiotopoulos 1987b, 1987a; Panagiotopoulos et al. 1988; Smit and de Smedt 1989): one of the simulation boxes represents the pore and the other is a gauge cell of limited capacity. Mass exchange between the two boxes is allowed; however, the box volumes are kept fixed. The limited capacity of the gauge cell constrains density fluctuations in the confined fluid and allows it to be kept in a state that would be unstable in contact with the bulk.

The gauge-cell method, with a suitably chosen gauge-cell volume, enables one to construct the full phase diagram of a confined fluid in the form of a van der Walls loop, which includes stable, metastable, and unstable equilibrium states. The phase coexistence is then determined by thermodynamic integration along the metastable and unstable regions of the phase diagram employing a Maxwell equal area construction (Fig. 1(a)):

$$\int_{\mu_e}^{\mu_{S_V}} \rho_A(\mu)\,d\mu + \int_{\mu_{S_L}}^{\mu_e} \rho_D(\mu)\,d\mu = \int_{\mu_{S_L}}^{\mu_{S_V}} \rho_U(\mu)\,d\mu, \quad (1)$$

where $\rho(\mu)$ is the adsorption isotherm expressed as a function of chemical potential μ, with subscripts A and D denoting vaporlike and liquidlike states on the adsorption and desorption branches, respectively, and U the unstable state achieved in the gauge-cell simulations. The regions in Fig. 1 along AV and DL are stable, those along VS_V and LS_L are metastable, and that along S_VS_L is unstable.

The gauge-cell method was first used to compute the adsorption isotherms and vapor–liquid equilibrium of Lennard–Jones (LJ) fluid in cylindrical pores (Neimark and Vishnyakov 2000), but quickly found applications in studies of phase behavior of more complex adsorbates and many other nanoscale systems. Recent examples include the adsorption and capillary condensation of nitrogen (Neimark and Vishnyakov 2000) and argon (Vishnyakov and Neimark 2001) and pore blocking effects (Vishnyakov and Neimark 2003b) in mesoporous cylindrical silica pores of MCM-41 and SBA-15 (Jorge and Seaton 2002a) type, water on carbons (Jorge and Seaton 2002b; Jorge et al. 2002), *n*-alkanes in carbon nanotubes (Jiang et al. 2004), embedding of phase equilibrium into methods for determination of nanotube size distribution (Kowalczyk et al. 2005), formation of liquid bridges/junctions in nanocapillaries (Vishnyakov and Neimark 2003a), bubble cavitation in stretched metastable liquid (Neimark and Vishnyakov 2005c), and droplet nucleation (Neimark and Vishnyakov 2005b).

In this paper, we present a modification of the gauge-cell method and apply it to the study of capillary phase transition of propane in single-walled carbon nanotubes of different diameters. After briefly reviewing the simulation details of the original gauge-cell method, we show how it can be simplified under the assumption that the equation of state for the gauge fluid is known. Finally, we examine the effect of propane confinement on its vapor–liquid coexistence curve and estimate its critical properties.

2 Method development

In the gauge-cell method, the chemical potential of a fluid confined to a finite volume V_p in the presence of an external potential is measured by considering its chemical

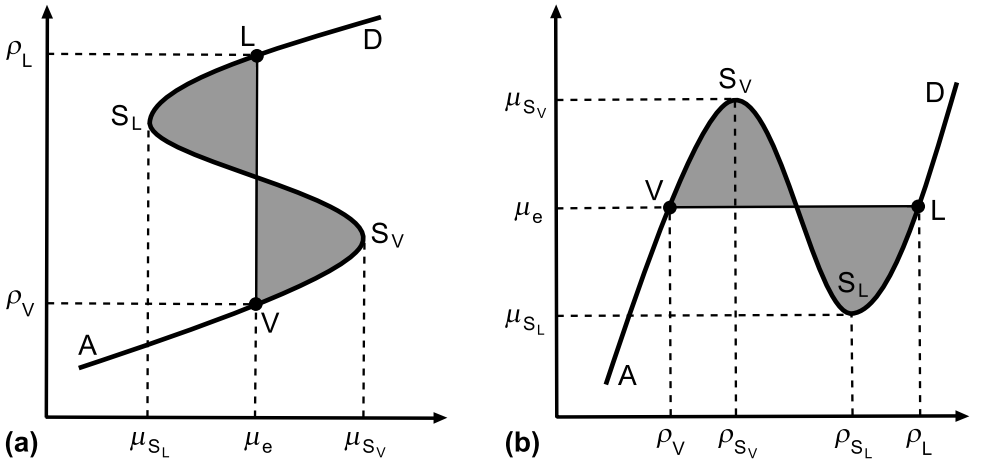

Fig. 1 Schematic of the Maxwell equal area construction, showing (**a**) the S-shaped adsorption isotherm $\rho(\mu)$ obtained by the gauge-cell method and (**b**) its inverse plot $\mu(\rho)$. The *solid curve* is the binodal curve. The regions of AV and DL are stable, of VS_V and LS_L are metastable, and of S_VS_L is unstable. The coexisting liquid–vapor phases, shown as *solid circles* L and V, and corresponding equilibrium chemical potential μ_e, are determined using the Maxwell equal area construction, which graphically corresponds to equality of the *two shaded areas*

Table 1 Alternative methods of implementing the particle exchange step and corresponding probability ratios

Method	Description	$\frac{\alpha_-(N_p+1)}{\alpha_+(N_p)}$	$\frac{\alpha_+(N_p-1)}{\alpha_-(N_p)}$
I	A box is chosen with equal probability and then a molecule is randomly selected for transfer to the other box.	$\frac{N_g}{N_p+1}$	$\frac{N_p}{N_g+1}$
II	A molecule is randomly selected regardless of its box and is transferred.	1	1

equilibrium with the fluid confined to a gauge cell of volume V_g, small enough to control the level of density fluctuations in the system. The simulation is performed similarly to the pore–fluid GEMC (Panagiotopoulos 1987a; Panagiotopoulos et al. 1988), in which both the total number of particles N and the volumes of the two boxes are fixed. That is, one deals with the canonical ensemble of particles, which are distributed between two mechanically isolated cells.

Given that the cell volumes are kept constant, the conditions of isothermal equilibrium are just the equality of chemical potentials in the confined and reference fluids. To achieve this in the gauge-cell method, transfers of particles between the two simulation boxes are attempted according to the acceptance rules of the GEMC method (Frenkel and Smit 1996).

The probability of accepting a move in which a particle is transferred from the gauge cell (g) to the pore cell (p) is given by

$$\mathrm{acc}(N_p \to N_p+1;\, N_g \to N_g-1) = \min\left\{1, \frac{\alpha_-(N_p+1)}{\alpha_+(N_p)}\frac{V_p}{V_g}\exp(-\beta\Delta U)\right\}, \quad (2)$$

where $\beta = 1/k_BT$, with k_B the Boltzmann's constant, $N_g = N - N_p$ and N_p are the number of molecules in the gauge cell and in the pore box, respectively, $\alpha_\pm(N_p)$ is the probability of changing the system from a state with N_p adsorbed particles to a new state with $N_p \pm 1$ adsorbed particles, and $\Delta U = \Delta U_g(\mathbf{r}^{N_g-1}) + \Delta U_p(\mathbf{r}^{N_p+1})$ is the total potential energy change resulting from the particle transfer. Analogously, if a particle moves from the adsorption box to the gauge cell, the acceptance probability is

$$\mathrm{acc}(N_p \to N_p-1;\, N_g \to N_g+1) = \min\left\{1, \frac{\alpha_+(N_p-1)}{\alpha_-(N_p)}\frac{V_g}{V_p}\exp(-\beta\Delta U)\right\}, \quad (3)$$

where $\Delta U = \Delta U_g(\mathbf{r}^{N_g+1}) + \Delta U_p(\mathbf{r}^{N_p-1})$ is again the total potential energy change resulting from the particle transfer.

As described in Table 1, the particle exchange step can be done in one of two ways. Each corresponds to a different method of selecting the particle to be transferred and, consequently, to a different expression for $\alpha_\pm(N_p)$. The choice between the two methods is a matter of convenience, although we tend to prefer method I which is the one used to obtain the simulation results presented in this work.

The equation of state for the gauge fluid, i.e., its chemical potential μ_g (or fugacity f_g) as a function of the number density ρ_g of molecules in the gauge cell, $\mu_g(\rho_g)$, is assumed known. For each simulated point in the isotherm, the mean numbers $\langle N_p\rangle$ and $\langle N_g\rangle$ of particles in the pore and gauge cells are computed, and the chemical potential of the pore fluid comprised of $\langle N_p\rangle$ particles is assumed to be equal to that of the gauge fluid at number density $\langle\rho_g\rangle$. For example, when the method was first applied to study vapor–liquid

equilibrium of LJ fluids in cylindrical pores (Neimark and Vishnyakov 2000; Vishnyakov and Neimark 2001), $\langle\rho_g\rangle$ was related to μ via the Johnson–Zollweg–Gubbins equation of state (Johnson et al. 1993). Another option is to estimate μ from the trial move of swapping a molecule between the two cells, using a procedure equivalent to the Widom test particle method (Widom 1963), as was done in the study of capillary phase transitions of n-alkanes in a carbon nanotube (Jiang et al. 2004). Often, the capillary phase transition occurs at low vapor pressure and in that case the ideal gas approximation holds.

To satisfy equality of chemical potentials between a multicomponent fluid subjected to an external potential in a box of fixed volume and fluid in a bulk box, either of fixed volume or at fixed pressure, we have recently developed acceptance rules for the trial move of particle exchange that reference the bulk system solely through the chemical potentials of the bulk mixture (Mota and Esteves 2004; Mota et al. 2005). In particular, we have shown that if an analytical equation of state for the fluid phase is known, it suffices to know the number of molecules of each species of fluid in the bulk cell to determine its potential energy U_g (the temperature and either the box volume or pressure are known and fixed). The individual number densities are the only state variables of the bulk box that must be updated during the course of the simulation. The resulting method (Mota and Esteves 2004) can be viewed as a hybrid Monte Carlo method, which incorporates features of both the GCMC (only the pore box is simulated) and GEMC techniques (the particle transfer move is retained).

By applying this concept to the original gauge-cell method we have obtained a simplified method for studying phase transitions in confined systems (Mota 2005a, 2005b). In essence, only the pore box undergoes configurational changes (molecule displacement, rotation, or conformational change), whose probability of acceptance is the same as for a conventional canonical simulation (Frenkel and Smit 1996):

$$\min\{1, \exp(-\beta\Delta U_p)\}, \tag{4}$$

where ΔU_p is the potential energy change resulting from the configurational move.

The acceptance probabilities for the particle transfer move, (2) and (3), are replaced by

$$\mathrm{acc}(N_p \to N_p + 1; N_g \to N_g - 1) = \min\left\langle 1, \frac{\alpha_-(N_p+1)}{\alpha_+(N_p)} \frac{\beta f_g(N_g) V_p}{N_g} \exp\{-\beta\Delta U_p(\mathbf{r}^{N_p+1})\}\right\rangle, \tag{5}$$

$$\mathrm{acc}(N_p \to N_p - 1; N_g \to N_g + 1) = \min\left\langle 1, \frac{\alpha_+(N_p-1)}{\alpha_-(N_p)} \frac{N_g+1}{\beta f_g(N_g+1) V_p} \exp\{-\beta\Delta U_p(\mathbf{r}^{N_p-1})\}\right\rangle. \tag{6}$$

where $f_g(N_g)$ is the fugacity of the bulk fluid at system temperature when its number density is $\rho_g(N_g) = N_g/V_g$ and $\Delta U_p(\mathbf{r}^{N_p\pm1})$ is the potential energy change in the pore box resulting from the particle transfer. Thus, the gauge cell gives a macroscopic description of the reference fluid which has a fluctuating density due to the particle exchange step.

Because of the absence of the energy fluctuations in the gauge cell that would result from configurational changes (molecule displacement, rotation or regrowth), the method is expected to give better statistics than the original method for dense vapor phases. Furthermore, it is very easy to adapt an existing GCMC code to handle the proposed scheme because it is unnecessary to add a second box (the gauge cell) to the simulation system. In fact, the only required change to the GCMC code is the replacement of the acceptance probabilities for the trial move of molecule exchange by those expressed in (5) and (6).

The proposed method is closely related to a recent modification of the gauge cell method proposed by Neimark and Vishnyakov (2005a), designed for chemical potential calculations in small, inhomogeneous and dense systems. Basically, the particles in the gauge cell are assumed as ideal, i.e. $U_g(\mathbf{r}^{N_g}) = 0$, and the acceptance probabilities for the particle transfer move, as given by (2) and (3), are simplified accordingly. This is equivalent to replacing f_g by ρ_g/β in the expressions for the acceptance probabilities of our method. The authors refer to this scheme as a mesoscopic canonical ensemble (MCE), since it is intermediate between the canonical ensemble (CE) and the (GCE) grand canonical ensemble, and the resulting computational method as the ideal-gas gauge cell method (IGGC). Given that our method does not necessarily consider the particles in the gauge cell as ideal, it can be regarded as a *nonideal* mesoscopic canonical ensemble and a generalization of the IGGC method.

In (Neimark and Vishnyakov 2005a), the IGGC method is illustrated on simulations of LJ fluid in spherical pores of different diameters to show its specifics and advantages, as compared to the Widom (1963) and original gauge-cell methods, in studies of phase equilibria and phase transitions in nanoscale systems. The authors also present a very interesting analysis of the conditions of extreme fluid confinement where inconsistency between the CE and the GCE is most pronounced. It is shown that the gauge cell method has practical advantages over the Widom for the calculation of the chemical potential in small, dense, inhomogeneous systems.

After determining the complete S-shaped isotherm $\rho(\mu)$ by the gauge-cell method, it is more convenient to work with the inverse adsorption isotherm $\mu(\rho)$, because it is a single-valued function of adsorbed density (Fig. 1(b)), whereas $\rho(\mu)$ is triple-valued for $\mu_{S_L} < \mu < \mu_{S_V}$ (Fig. 1(a)). The

Maxwell rule of equal areas, as expressed by (1), can be written for $\mu(\rho)$ as

$$\int_{\rho_V}^{\rho_L} \mu(\rho)\,\mathrm{d}\rho = \mu_e(\rho_L - \rho_V). \tag{7}$$

In practice, we replace the discrete gauge-cell simulation data by an approximating smoothing spline $\tilde{\mu}(\rho)$ over a range of adsorbed densities that includes $[\rho_V, \rho_L]$. This is a continuous function that can be easily differentiated and integrated. It is then easy to build a function $\tilde{\rho}_L(\rho_V)$ that for a given ρ_V value along AS_V, corresponding to a low-density vaporlike state, returns the ρ_L value for the high-density liquidlike state characterized by the same chemical potential. This is equivalent to finding the zero of

$$\tilde{\mu}(\rho) - \tilde{\mu}(\rho_V), \quad \rho > \rho_{S_L}, \tag{8}$$

for a given value of ρ_V, using a suitable root-finding algorithm; for this purpose we use a combination of bisection and the Newton–Raphson method. This is the inner loop of our algorithm. Then, using Brent's root-finding method (this method only requires function evaluations) in an outer loop we solve

$$\int_{\rho_V}^{\tilde{\rho}_L(\rho_V)} \tilde{\mu}(\rho)\,\mathrm{d}\rho = \tilde{\mu}(\rho_V)\cdot(\tilde{\rho}_L(\rho_V) - \rho_V), \tag{9}$$

for $\rho_V < \rho_{S_V}$ to get the equilibrium chemical potential $\tilde{\mu}_e \equiv \tilde{\mu}(\rho_V)$. The numerical methods for root finding used in this work were adapted from (Press et al. 1989).

In the next section our method is validated and successfully applied to study the capillary phase transition of propane in open-ended single-walled carbon nanotubes of different diameters. To enhance the sampling of confined propane molecules in the hollow space of the nanotube we resort to the configurational-bias scheme (Siepmann and Frenkel 1992; Frenkel et al. 1992; de Pablo et al. 1992; Frenkel and Smit 1996) for molecule insertion/deletion and regrowth.

3 Simulation details

Fluid–fluid interaction is modeled by the Lennard–Jones (LJ) potential

$$u_{ij}(r) = 4\epsilon_{ij}[(\sigma_{ij}/r)^{12} - (\sigma_{ij}/r)^6], \tag{10}$$

as is the interaction between individual atoms of the pore wall and each adsorbate site. In (10), r is the intermolecular distance; the well depths, ϵ_i/k_B, and collision diameters, σ_i, used are given in Table 2. The cross terms were obtained using the standard Lorenz–Berthelot combining rules: $\epsilon_{ij} = (\epsilon_i\epsilon_j)^{1/2}$ and $\sigma_{ij} = (\sigma_+\sigma_j)/2$.

Table 2 Lennard–Jones potential parameters

Site	ϵ/k_B (K)	σ (Å)
Wall (SWNT)	28.0	3.40
CH_3	98.0	3.75
CH_2	46.0	3.95

The force field adopted for propane is the transferable potential for phase equilibria (TraPPE) (Martin and Siepmann 1998), which is based on an united-atom model where each CH_3 or CH_2 group is treated as a single interaction site. Adjacent pseudo-atoms of a propane molecule are connected by a rigid bond length of 1.54 Å; the harmonic bond-bending potential $U_{bend}(\theta)$, along the three pseudo-atoms, is governed by

$$U_{bend} = k_\theta(\theta - \theta_0)^2/2, \tag{11}$$

with force constant $k_\theta/k_B = 62\,500$ K rad^{-2} and equilibrium bending angle $\theta_0 = 114°$.

For a fluid interaction site located at a nearest distance δ from the central axis of the cylindrical pore, an effective potential $U_{sf}(\delta)$ is developed by integrating the LJ solid–fluid potential u_{sf} over the positions of all wall atoms in a cylinder of infinite length:

$$\begin{aligned} U_{sf}(\delta) &= 4\rho_s R\int_0^{+\infty}\int_0^{\pi} u_{sf}(r)\,\mathrm{d}\theta\,\mathrm{d}z, \\ r^2 &= R^2 + \delta^2 + z^2 - 2\delta R\cos\theta, \end{aligned} \tag{12}$$

where R is the pore radius, z is the distance along the cylinder axis, θ is the radial angle, and $\rho_s = 0.382$ Å^2 is the atomic surface density of the pore wall. By integrating over z and θ, (12) is reduced to a one-dimensional potential which depends on δ only (Tjatjopoulos et al. 1988):

$$\begin{aligned} U_{sf}(\delta) = \pi^2\rho_s\epsilon_{sf}\sigma_{sf}^2\Bigg\{ &\frac{63}{32}\frac{R-\delta}{\sigma_{sf}}\left(1+\frac{\delta}{R}\right)^{-10} \\ &\times F\left[-\frac{9}{2},-\frac{9}{2},1;\left(\frac{\delta}{R}\right)^2\right] \\ &-3\frac{R-\delta}{\sigma_{sf}}\left(1+\frac{\delta}{R}\right)^{-4} \\ &\times F\left[-\frac{3}{2},-\frac{3}{2},1;\left(\frac{\delta}{R}\right)^2\right]\Bigg\}, \end{aligned} \tag{13}$$

where $F(\alpha,\beta,\gamma;\delta)$ is the hypergeometric function. To speedup the calculation of U_{sf}, (13) was tabulated on a grid with 31 knots equally spaced in δ^2. During the simulations U_{sf} was reconstructed from the tabulated information using cubic Hermite polynomial interpolation.

Attempts to apply standard techniques of molecule insertion/deletion, or molecule transfer between boxes, to large sorbates, or to systems in which the sorbates fit very tightly into the pores, result in very low acceptance rates of those steps needed to correctly sample the ensemble. Furthermore, even for a simple geometry such as that of a cylindrical pore not all portions of its accessible space are equally favorable; there exist preferred regions in which sorbate molecules are localized. This information can be incorporated into a simulation if insertions are not attempted randomly throughout the volume, but rather are performed such that sorbates are inserted preferentially into the most favorable locations of the pore space. This provides a substantial improvement in the efficiency of the simulation compared to a traditional one.

To enhance the sampling of configurational space and increase the acceptance rate of the particle insertion/removal step for the simulations of propane adsorption, we resort to configurational-bias sampling techniques (Siepmann and Frenkel 1992; Frenkel et al. 1992; de Pablo et al. 1992; Frenkel and Smit 1996). In the configurational-bias method a flexible molecule is grown atom-by-atom towards energetically favorable conformations, leading to a scheme which is orders of magnitude more efficient than the traditional method of random growth. For the placement of the first CH_3 pseudo-atom of propane, $k_1 = 10$ random positions in the simulation box are generated and one is selected with a probability $\exp(-\beta U_{1,i}^{\text{ext}})/\sum_j \exp(-\beta U_{1,j}^{\text{ext}})$, where $U_{1,j}^{\text{ext}}$ is the external energy of the CH_3 pseudo-atom at the jth trial position interacting with the pore and with the pseudo-atoms of the other propane molecules. For each of the remaining two pseudo-atoms ($m = 2, 3$) of the molecule, $k_m = 5$ trial positions are generated with a probability proportional to $\exp(-\beta U_{m,j}^{\text{int}})$. These positions are distributed on the surface of a sphere centered on the previously inserted pseudo-atom of the molecule and whose radius is equal to the bond length. Each set of k_m trial orientations is generated using the internal part of the potential $U_{m,j}^{\text{int}}$, whose probability depends on which type of pseudo-atom is being inserted: for the second atom ($m = 2$) the internal potential energy is zero and, as a result, the trial positions are randomly distributed on a sphere; for the third atom ($m = 3$) the internal potential energy includes bond bending and the trial positions are distributed on the edge of the disk which forms the base of a cone with apex at the center of the previously inserted bead and slant height equal to the bond length. For each trial position j ($j = 1, \ldots, k_m$) the external energy $U_{m,j}^{\text{ext}}$ is calculated for interaction with the nanotube, and with the atoms of the other propane molecules. From among the k_m trial positions, one is selected with a probability $\exp(-\beta U_{m,i}^{\text{ext}})/\sum_j \exp(-\beta U_{m,j}^{\text{ext}})$. During this growth process a bias is introduced and is removed by adjusting the acceptance rules.

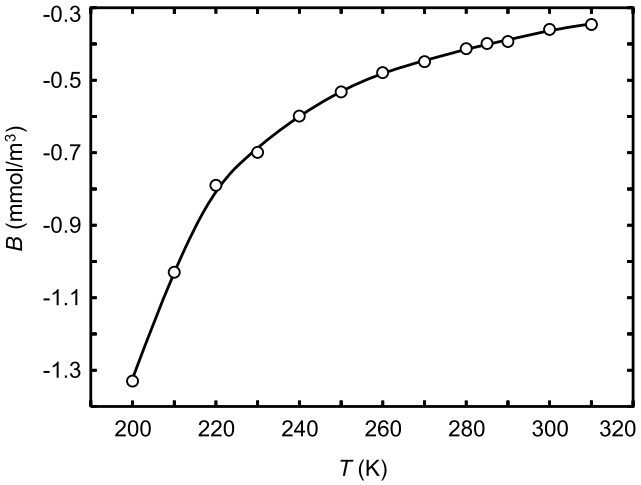

Fig. 2 Second virial coefficient B of bulk propane vapor as a function of temperature, determined from GCMC simulation data for the TraPPE force field

Besides the usual trial step of molecule insertion/deletion, whose acceptance rate is enhanced by resorting to configurational-bias techniques, three additional types of Monte Carlo (MC) moves involving only individual molecules are necessary to sample the internal configuration of the simulation box: translation, rotation about the center-of-mass, and configurational-bias partial regrowth to change the internal conformation of the molecule. Each run was equilibrated for 2×10^4 Monte Carlo cycles followed by an equal number of Monte Carlo cycles for the production period. Each cycle consists of $0.8N_{\text{p}}$ attempts to translate a randomly selected molecule, $0.2N_{\text{p}}$ trial rotations, $0.2N_{\text{p}}$ attempts to change the conformation of a molecule using configurational-bias partial regrowth, and $\max\{20, 0.2N_{\text{p}}\}$ molecule insertion/deletion steps. Here, N_{p} is the number of molecules in the pore box at the beginning of each cycle. The maximum displacement for translation and angle for rotation were adjusted during the equilibration phase to give a 50% acceptance rate. Standard deviations of the ensemble averages were computed by breaking the production run into five blocks.

For the temperature range considered in this study, the equation of state for bulk propane vapor is well described by the truncated Virial equation of state (Reid et al. 1988):

$$f_{\text{g}} = \frac{\rho_{\text{g}}/\beta}{1 - \rho_{\text{g}} B} \exp\left(\frac{\rho_{\text{g}} B}{1 - \rho_{\text{g}} B}\right). \tag{14}$$

The value of the second Virial coefficient B for each temperature was evaluated by nonlinear least-squares fitting of (14) to simulated data (f, ρ_{g}) obtained from a series of inexpensive GCMC simulations on the bulk fluid. The temperature dependence of B is displayed in Fig. 2.

4 Results and discussion

Figure 3 shows isotherms for propane confined in open-ended single-walled carbon nanotubes with three different diameters: 27.12 Å, 33.90 Å and 40.69 Å, corresponding to chirality vectors (20, 20), (25, 25) and (30, 30), respectively. These are the nanotube diameters selected for this study, which we believe to be sufficient to get a qualitative picture of the influence of nanotube size on the capillary phase transition; the extension to other nanotubes would be straightforward. The temperature range analyzed for each nanotube diameter covers both subcritical conditions, for determining the binodal curve, and a few values above the capillary critical temperature.

The open circles in Fig. 3 were obtained by the original gauge-cell method, whereas the solid ones were obtained by the present method. It is clear that both methods give identical results to within statistical error. As discussed above, a smooth isotherm curve is obtained by fitting an approximating smoothing spline to the corresponding set of simulated data obtained by the gauge-cell method. The quality of the fit is an additional proof of small scattering of the simulation points. The dashed part of the curve locates the metastable and unstable regions of the isotherm, which separate the vaporlike and liquidlike stable regions. The vertical lines show the location of vapor–liquid coexistence calculated by the Maxwell rule of equal areas.

The size of the van der Walls loop is reduced in size on increasing temperature and vanishes completely when the capillary critical temperature of propane in the nanotube is surpassed. Above the capillary critical temperature, the isotherm is a monotonic function of the chemical potential and it is no longer possible to distinguish between vaporlike and liquidlike phases. This effect is shifted to lower temperatures as the nanotube diameter is decreased. For a sufficiently small nanotube the system would approach one-dimensional behavior and there would be no phase transition.

Figure 4 shows radial density profiles for the center-of-mass of confined propane in the three different sized nanotubes for selected states of the S-shaped isotherm. Radial profiles A and C correspond to vaporlike and liquidlike coexisting states, respectively, whereas the B profile is representative of the unstable state for $\mu = \mu_e$ accessed by the gauge-cell method. For the three different nanotubes there is the formation of a dense monolayer near the tubular wall, followed by multilayer adsorption for the denser states as one moves closer to the nanotube center. Because of geometric impediment, the number of layers decreases with decreasing tube diameter. The vaporlike state is characterized by two well-defined monolayers adsorbed on the wall and a smooth inner core with low vapor density. The stable liquidlike state has a similar well-pronounced bilayer structure

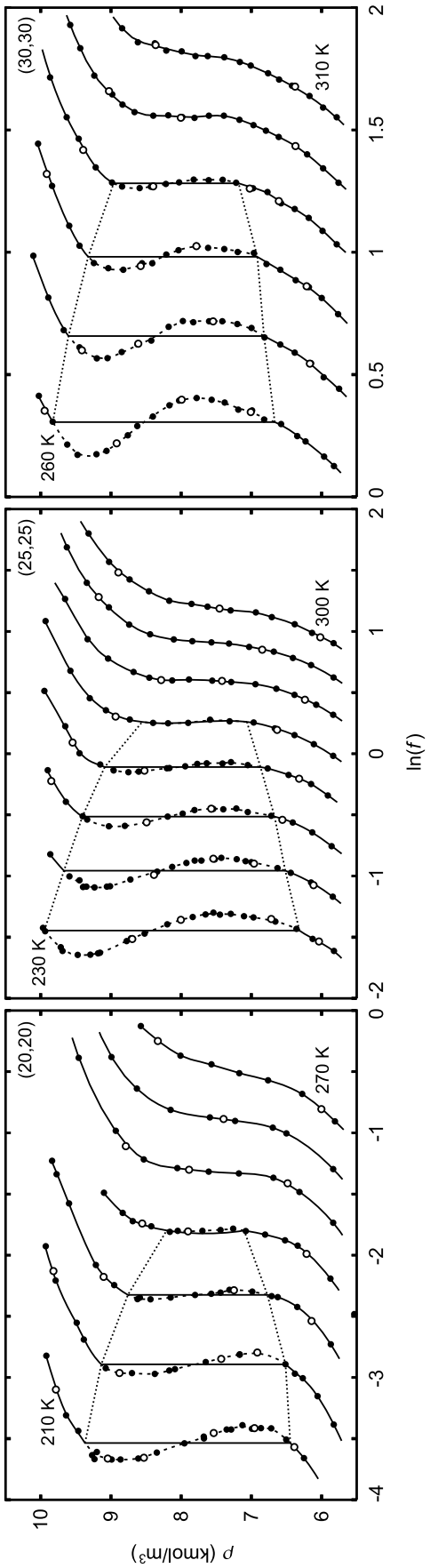

Fig. 3 Adsorption isotherms for propane confined inside (*20,20*), (*25,25*) and (*30,30*) open-ended nanotubes at various temperatures. In each plot the isotherms are shown in temperature steps of 10 K. The *open circles* were obtained by the original gauge-cell method, whereas the *solid circles* were obtained by the simplified version of the method proposed in this work. The *vertical line* shows the location of vapor–liquid coexistence calculated by the Maxwell rule of equal areas. The *dotted curve* is the binodal curve. Also shown are the isotherm curves obtained by fitting an approximating smoothing spline to each set of simulated isotherm data. The *dashed part* of each isotherm locates the metastable and unstable regions, which separate the vaporlike and liquidlike stable regions (solid segments)

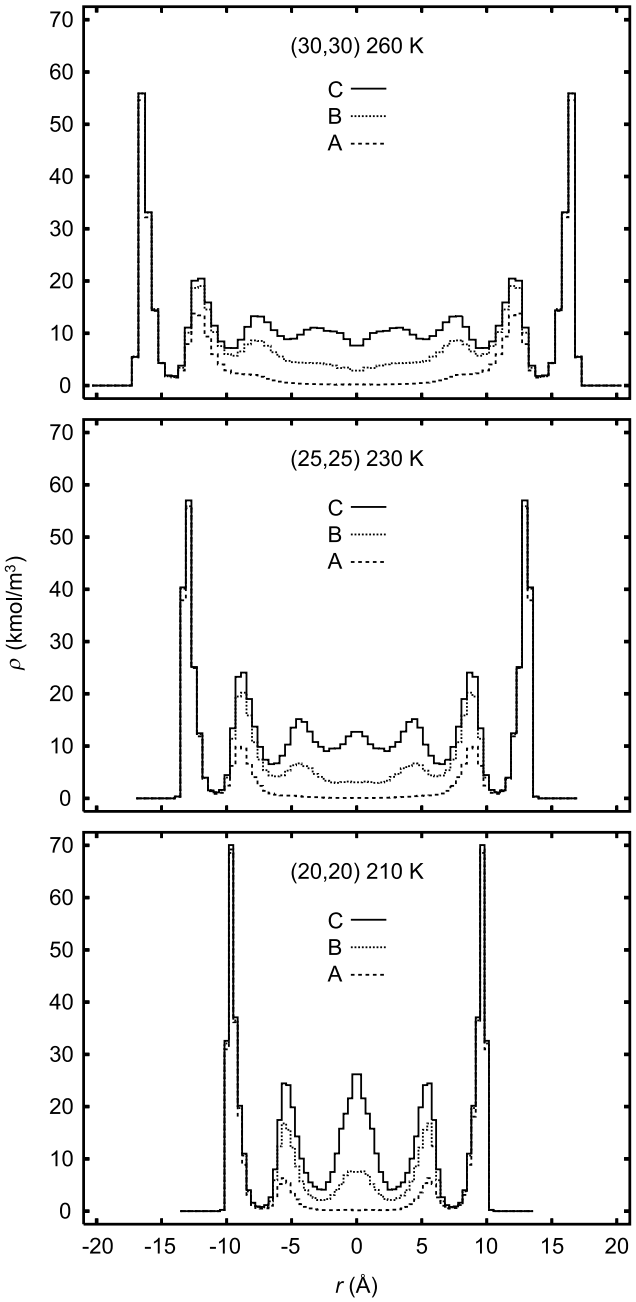

Fig. 4 Density profiles of confined propane in the three different sized nanotubes for selected thermodynamic conditions identified by letters A, B and C. A and C are vaporlike and liquidlike states at the vapor–liquid coexistence, respectively; B is the unstable state at $\mu = \mu_e$ accessed by the gauge-cell method

near the wall, but the inner core is replaced by a multilayer structure. With an increase in tube diameter, the core layering becomes less pronounced and approaches the smooth structure and density of the bulk liquid at the same temperature. The unstable state (B) at the same chemical potential has an intermediate structure between those of the vaporlike and liquidlike states.

Notice that due to the strong wall field the densities of the first layer in the three states of Fig. 4 are practically equal and considerably higher than that of the bulk liquid at the same temperature. Therefore, phase coexistence cannot be discriminated from the structure of the monolayer adsorbed on the wall and, unless a tube is large enough to accommodate more than one layer, there will be no phase transition.

Despite being computationally more expensive than the pore–pore GEMC, the gauge-cell method has the advantage of providing both sub- and supercritical data that can be employed for estimation of critical properties by interpolation rather than by extrapolation. This feature has not been put into evidence in previous works where the gauge-cell method has been employed. Notice that under subcritical conditions the inverse adsorption isotherms $\mu(\rho)$ plotted in Fig. 3 have two points with zero slope,

$$\left(\frac{\mathrm{d}\mu}{\mathrm{d}\rho}\right)_{\rho=\rho_{S_V}} = \left(\frac{\mathrm{d}\mu}{\mathrm{d}\rho}\right)_{\rho=\rho_{S_L}} = 0, \tag{15}$$

and an inflection point with negative slope located between ρ_{S_V} and ρ_{S_L}:

$$\left(\frac{\mathrm{d}^2\mu}{\mathrm{d}\rho^2}\right)_{\rho=\rho'} = 0,$$
$$\left(\frac{\mathrm{d}\mu}{\mathrm{d}\rho}\right)_{\rho=\rho'} < 0, \quad \rho_{S_V} < \rho' < \rho_{S_L}. \tag{16}$$

As the subcritical temperature is increased, both the density difference $\rho_{S_L} - \rho_{S_V}$ and chemical potential difference $\mu_{S_L} - \mu_{S_V}$ decrease and vanish at the critical point. Also, from (15) and (16) it follows that at the capillary critical point

$$\left(\frac{\mathrm{d}\mu}{\mathrm{d}\rho}\right)_{\rho=\rho_c} = 0. \tag{17}$$

Above the critical temperature, $\mu(\rho)$ becomes a monotonically increasing function of ρ but maintains the inflection point which now has positive slope:

$$\left(\frac{\mathrm{d}^2\mu}{\mathrm{d}\rho^2}\right)_{\rho=\rho'} = 0, \qquad \left(\frac{\mathrm{d}\mu}{\mathrm{d}\rho}\right)_{\rho=\rho'} > 0. \tag{18}$$

This suggests that the critical point can be estimated by interpolation of sub- and supercritical values of $(\mathrm{d}\mu/\mathrm{d}\rho)_{\rho=\rho'}$ to determine where $(\mathrm{d}\mu/\mathrm{d}\rho)_{\rho=\rho'} = 0$. This is easily done in the present work because the approximating smoothing spline $\tilde{\mu}(\rho)$ that we employ to generate a continuous approximation of the isotherm is a C^2 continuous function whose first and second derivatives can be calculated analytically.

Figure 5 shows the estimation of critical temperature for the three tube diameters by the aforementioned procedure.

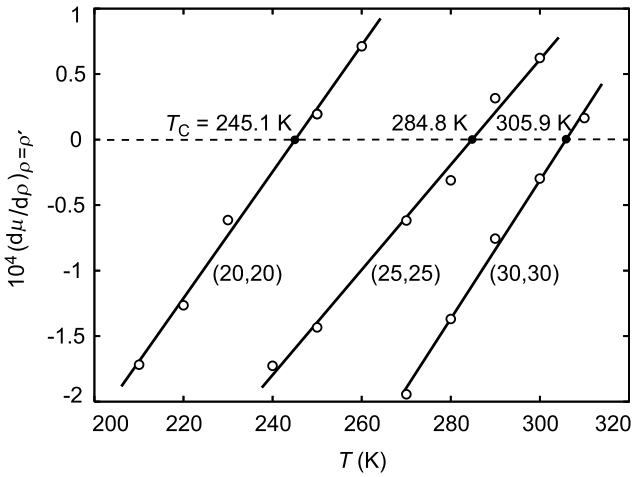

Fig. 5 Estimation of capillary critical temperature by interpolation of the slope $(\mathrm{d}\mu/\mathrm{d}\rho)_{\rho=\rho'}$ of the S-shaped inverse isotherm at the inflection point $\rho'(T)$ for both sub- and supercritical data

The values of $(\mathrm{d}\mu/\mathrm{d}\rho)_{\rho=\rho'}$ show little scattering and a linear trend in the vicinity of the critical point is clearly observed. The error in the estimated values of T_c is about ± 0.2 K.

The coexistence data for each nanotube diameter are fitted to a theoretical binodal curve of the form (Domb 1996)

$$\rho_{\pm} = \rho_c + A(T_c - T) \pm B(T_c - T)^{\beta}, \tag{19}$$

where $+$ denotes liquidlike phase, $-$ denotes vaporlike phase, and T_c is the estimated value of critical temperature obtained by interpolation of the gauge-cell data. This procedure allows us to estimate the critical density ρ_c, which together with the amplitudes A and B and critical exponent β are treated as adjustable parameters. In principle, ρ_c could also be determined by the aforementioned method employed to estimate T_c and, in that case, (19) would only be employed for approximating the coexistence data and providing the critical exponent. In practice, however, (19) provides a more robust estimation of ρ_c because $(\mathrm{d}\mu/\mathrm{d}\rho)_{\rho=\rho'}$ is determined with considerable less error than ρ' due to the flatness of $\mu(\rho)$ near the inflection point.

To simultaneously determine the unknown parameters of (19), it is rewritten as

$$\rho(\eta, T) = \rho_c + A(T_c - T) + B\eta(T_c - T)^{\beta}, \tag{20}$$

where $\eta = -1$ if the coexisting density is vaporlike (ρ_-) and $\eta = +1$ if it is liquidlike (ρ_+). The parameters are then estimated by nonlinear least-squares fitting of the simulated coexistence data for the predetermined value of T_c.

The average over the values of critical exponent obtained for the three tube sizes is $\bar{\beta} = 0.5 \pm 0.1$, which is consistent with a classical mean-field behavior. This is expected, given that density fluctuations are constrained by the finite size of the two simulation boxes employed in the gauge cell method. Close to the critical point our simulation system is too small to accommodate long-range fluctuations and, as a consequence, mean field behavior should be observed.

The densities plotted in Fig. 3 are based on a pore volume defined by the skeletal diameter D of the nanotube, i.e. the distance between the centers of opposing carbon atoms in the cylindrical wall. This definition of tube diameter is convenient from the point of view of molecular modeling, yet inconsistent with the rigorous thermodynamic setting of the fluid/solid boundary because it does not provide the zero excess mass/volume of solid (Kaneko et al. 1994). The radial density profiles plotted in Fig. 4 clearly show a nonnegligible annular volume adjacent to the wall that is inaccessible to sorbate molecules due to the strong short-ranged repulsive potential. Since it is difficult to unambiguously define the internal accessible volume of a micropore for a chain molecule, we take as reference value for the thickness of the repulsive annular layer the largest distance from the wall at which the radial density profile for the center-or-mass obtained at the highest chemical potentials is zero ($\approx$3.15 Å). Thus, the net internal volume occupied by propane in the nanotube is proportional to $(D - 2 \times 3.15)^2$, whereas the skeletal volume of the nanotube scales with D^2. Our analysis of the vapor–liquid phase transition of confined propane is based not only on primitive density ρ obtained by simulation but also on an effective density

$$\rho^* = \rho\left(\frac{D}{D - 2 \times 3.15}\right)^2, \tag{21}$$

which reflects the fact that not all of the hollow space of the nanotube is accessible to the propane molecules. This allows for a realistic comparison with bulk densities.

The binodal curves for the three different nanotubes are plotted in Fig. 6 and compared to that of bulk propane obtained using GEMC simulations (Martin and Siepmann 1998). The solid lines are the fits of (19) to the simulated coexistence densities, represented as solid circles, based on the skeletal volume of the nanotube, whereas the dotted lines are the same data scaled by the factor $D^2/(D - 2 \times 3.15)^2$. It is seen that the confinement of propane in the carbon nanotubes decreases its capillary critical temperature, increases its critical density and narrows its binodal curve. The critical temperature is reduced and the binodal curve is narrowed with decreasing tube diameter until the system approaches one-dimensional behavior. Overall, the confinement causes a considerable increase of the density ρ_V of the vaporlike phase and a decrease of skeletal-based density ρ_L of the liquidlike phase in the tube compared to those of the corresponding coexisting bulk phases at the same temperature. However, when the density is scaled by the ratio of skeletal-to-accessible pore volumes it is seen that the confinement increases the liquidlike density ρ_L^* above that of the bulk

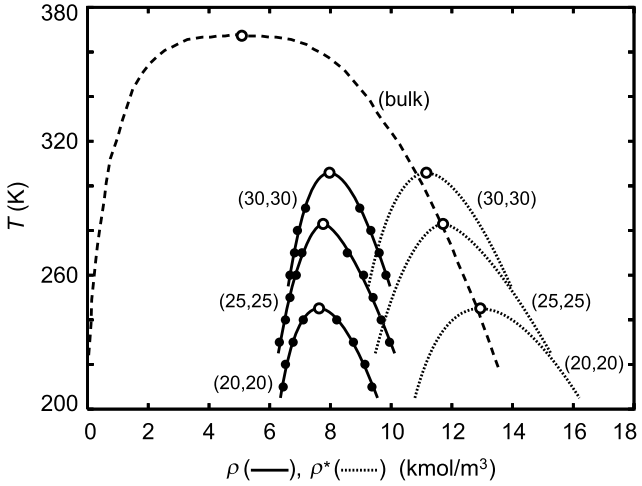

Fig. 6 Coexistence curves for confined (*solid and dotted lines*) and bulk (*dashed line*) propane. The latter was reproduced from the GEMC simulated data of (Martin and Siepmann 1998). The *solid circles* represent the vaporlike–liquidlike coexistence phases of confined propane determined by the Maxwell equal area construction applied to the gauge-cell simulation data. The *open circles* are estimates of the critical point for each tube diameter. The *dotted lines* are obtained by scaling the density according to $\rho^*/\rho = D^2/(D - 2 \times 3.15)^2$

liquid at the same temperature. The effect of tube diameter on critical density ρ_c is less clear, and probably larger nanotubes should be studied to get a better defined trend. On the other hand, the dependence of ρ_c^* on tube diameter is better defined. The values of ρ_c^* for the three nanotubes are very close to the densities of the bulk liquid at the same temperatures and decrease with increasing tube diameter.

5 Conclusions

Consistent results were obtained between the original gauge-cell method and the modified version proposed in this work. By using an analytical equation of state for the vapor phase, the acceptance rule for the trial move of particle exchange can be modified to reference the bulk system through its chemical potential. It is very easy to adapt an existing GCMC code to handle the proposed scheme because it is unnecessary to add a second box to the simulation system. It is shown that the critical temperature can be estimated by interpolation of sub- and supercritical values of the slope of the inverse isotherm at the inflection point.

The capillary phase transition of propane in single-walled carbon nanotubes has been investigated using the proposed method. To enhance the sampling of confined propane molecules in the hollow space of the nanotubes the configurational-bias scheme has been employed. The analysis of vapor–liquid phase transition is based both on primitive density ρ and on its scaled value ρ^* to reflect the fact that not all of the hollow space of the nanotube is accessible to the confined fluid. By comparing the simulated coexistence curves for different tube diameters, conclusions can be drawn as to the influence of this geometrical parameter on the binodal curve and capillary critical parameters of confined propane.

References

Agnihotri, S., Mota, J.P.B., Rostam-Abadi, M., Rood, M.J.: Structural characterization of single-walled carbon nanotube bundles by experiment and molecular simulation. Langmuir **21**, 896 (2005a)

Agnihotri, S., Rood, M.J., Rostam-Abadi, M.: Adsorption equilibrium of organic vapors on single-walled carbon nanotubes. Carbon **43**, 2379 (2005b)

Alvarez, M., Levesque, D., Weis, J.-J.: Monte Carlo approach to the gas–liquid transition in porous materials. Phys. Rev. E **60**, 5495 (1999)

Baughman, R.H., Zakhidov, A.A., Heer, W.A.: Carbon nanotubes—the route toward applications. Science **297**, 787 (2002)

Brovchenko, I., Geiger, A., Oleinikova, A.: Phase equilibria of water in cylindrical nanopores. Phys. Chem. Chem. Phys. **3**, 1567 (2001)

Brovchenko, I., Geiger, A., Oleinikova, A.: Water in nanopores, I: Coexistence curves from Gibbs ensemble Monte Carlo simulations. J. Chem. Phys. **120**, 1958 (2004a)

Brovchenko, I., Geiger, A., Oleinikova, A.: Water in nanopores, II: The liquidvapour phase transition near hydrophobic surfaces. J. Phys. Condens. Matter **16**, S5345 (2004b)

Calbi, M.M., Cole, M.W., Gatica, S.M., Bojan, M.J., Stan, G.: Condensed phases of gases inside nanotube bundles. Rev. Mod. Phys. **73**, 857 (2001)

Cinke, M., Li, J., Bauschlicher, C.W., Ricca, A., Meyyappan, M.: CO2 adsorption in single-walled carbon nanotubes. Chem. Phys. Lett. **376**, 761 (2003)

Darkrim, F.L., Malbrunot, P., Tartaglia, G.P.: Review of hydrogen storage by adsorption in carbon nanotubes. Int. J. Hydrog. Energy **27**, 193 (2002)

de Pablo, J.J., Laso, M., Suter, U.W.: Simulation of polyethylene above and below the melting point. J. Chem. Phys. **96**, 2395 (1992)

Domb, C.: The Critical Point: A Historical Introduction to the Modern Theory of Critical Phenomena. Taylor & Francis, London (1996)

Duren, T., Keil, F.J.: Molecular modeling of adsorption in carbon nanotubes. Chem. Eng. Technol. **24**, 698 (2001)

Evans, R.: Fluids adsorbed in narrow pores: phase equilibria and structure. J. Phys. Condens. Matter **2**, 8989 (1990)

Frenkel, D., Smit, B.: Understanding Molecular Simulation. Academic, New York (1996)

Frenkel, D., Mooij, G.C.A.M., Smit, B.: Novel scheme to study structural and thermal properties of continuously deformable molecules. J. Phys. Condens. Matter **4**, 3053 (1992)

Gelb, L.V., Gubbins, K.E.: Kinetics of liquid–liquid phase separation of a binary mixture in cylindrical pores. Phys. Rev. E **55**, R1290 (1997a)

Gelb, L.V., Gubbins, K.E.: Liquid–liquid phase separation in cylindrical pores: Quench molecular dynamics and Monte Carlo simulations. Phys. Rev. E **56**, 3185 (1997b)

Gelb, L.V., Gubbins, K.E., Radhakrishnan, R., Sliwinska-Bartkowiak, M.: Phase separation in confined system. Rep. Prog. Phys. **62**, 1573 (1999)

Harrys, P.F.J.: Carbon Nanotubes and Related Structures: New Materials for the 21st Century. Cambridge University Press, Cambridge (1999)

Gozdz, W.T., Gubbins, K.E., Panagiotopoulos, A.Z.: Liquid–liquid phase transitions in pores. Mol. Phys. **84**, 825 (1995)

Heffelfinger, G.S., van Swol, F., Gubbins, K.E.: Liquid–vapor coexistence in a cylindrical pore. Mol. Phys. **61**, 1381 (1987)
Heffelfinger, G.S., van Swol, F., Gubbins, K.E.: Adsorption hysteresis in narrow pores. J. Chem. Phys. **89**, 5202 (1988)
Hilding, J., Grulke, E.A., Sinnot, S.B., Qian, D., Andrews, R., Jagtoyen, M.: Sorption of butane on carbon multiwall nanotubes at room temperature. Langmuir **17**, 7540 (2001)
Hinds, B.J., Chopra, N., Rantell, T., Andrews, R., Gavalas, V., Bachas, L.G.: Aligned multiwalled carbon nanotube membranes. Science **303**, 62 (2004)
Jiang, J., Sandler, S.I.: Nitrogen adsorption on carbon nanotube bundles: Role of the external surface. Phys. Rev. B **68**, 245412 (2003)
Jiang, J., Sandler, S.I., Smit, B.: Capillary phase transitions of n-alkanes in a carbon nanotube. Nano Lett. **4**, 241 (2004)
Jiang, J., Sandler, S.I., Schenk, M., Smit, B.: Adsorption and separation of linear and branched alkanes on carbon nanotube bundles from configurational-bias Monte Carlo simulation. Phys. Rev. B **72**, 045447 (2005)
Johnson, J.K., Zollweg, J.A., Gubbins, K.E.: The Lennard–Jones equation of state revisited. Mol. Phys. **78**, 591 (1993)
Jorge, M., Seaton, N.A.: Molecular simulation of phase coexistence in adsorption in porous solids. Mol. Phys. **100**, 3803 (2002a)
Jorge, M., Seaton, N.A.: Characterisation of the surface chemistry of activated carbon by molecular simulation of water adsorption. Stud. Surf. Sci. Catal. **144**, 131 (2002b)
Jorge, M., Schumacher, C., Seaton, N.A.: Simulation study of the effect of the chemical heterogeneity of activated carbon on water adsorption. Langmuir **18**, 9296 (2002)
Kaneko, K., Cracknell, R.F., Nicholson, D.: Nitrogen adsorption in slit pores at ambient temperatures: comparison of simulation and experiment. Langmuir **10**, 4606 (1994)
Kowalczyk, P., Holyst, R., Tanaka, H., Kaneko, K.: Distribution of carbon nantube sizes from adsorption measurements and computer simulation. J. Phys. Chem. B **109**, 14659 (2005)
Kuznetsova, A., Yates, J.T., Liu, J., Smalley, R.E.: Physical adsorption of xenon in open single walled carbon nanotubes: observation of a quasi-one-dimensional confined Xe phase. J. Chem. Phys. **112**, 9590 (2000)
Lastoskie, C., Gubbins, K.E., Quirke, N.: Pore-size distribution analysis of microporous carbons—a density-functional theory approach. J. Phys. Chem. **97**, 4786 (1993)
Levesque, D., Gicquel, A., Darkrim, F.L., Kayiran, S.B.: Monte Carlo simulations of hydrogen storage in carbon nanotubes. J. Phys. Condens. Matter **14**, 9285 (2002)
Long, R.Q., Yang, R.T.: Carbon nanotubes as superior sorbent for dioxin removal. J. Am. Chem. Soc. **123**, 2058 (2001)
Maddox, M.W., Gubbins, K.E.: Molecular simulation of fluid adsorption in buckytubes. Langmuir **11**, 3988 (1995)
Martin, M.G., Siepmann, J.I.: Transferable potentials for phase equilibria. 1. United-atom description of n-alkanes. J. Phys. Chem. B **102**, 2569 (1998)
McGrother, S.C., Gubbins, K.E.: Constant pressure Gibbs ensemble Monte Carlo simulations of adsorption into narrow pores. Mol. Phys. **97**, 955 (1999)
Mota, J.P.B.: Efficient gauge-cell method for studying capillary phase transitions in nanoporous materials. In: Proc. 7th Meeting of Division of Catalysis and Porous Materials, p. 85. Portuguese Chemical Society, Lisbon (2005a)
Mota, J.P.B.: Efficient gauge-cell method for studying capillary phase transitions in carbon nanoporores. In: Proc. Carbon 2005 Conf., Gyeongju, Korea, July 2005. Paper P09-01 (2005b)
Mota, J.P.B., Esteves, I.A.A.C.: Molecular simulation of adsorption processes. 1. Isothermal stirred-tank adsorber. Mol. Simul. **30**, 387 (2004)
Mota, J.P.B., Esteves, I.A.A.C., Rodrigues, R.C.R., Formiga, N.F.C.: Molecular simulation of gas separation by equilibrium-based adsorption processes. Adsorption **11**, 319 (2005)
Muris, M., Dufau, N., Bienfait, M., Pavlovsky, N.D., Grillet, Y., Palmari, J.P.: Methane and krypton adsorption on single-walled carbon nanotubes. Langmuir **16**, 7019 (2000)
Neimark, A.V., Vishnyakov, A.: Gauge cell method for simulation studies of phase transitions in confined systems. Phys. Rev. E **62**, 4611 (2000)
Neimark, A.V., Vishnyakov, A.: A simulation method for the calculation of chemical potential in small, inhomogeneous, and dense systems. J. Chem. Phys. **122**, 234108 (2005a)
Neimark, A.V., Vishnyakov, A.: A Monte Carlo study of droplet nucleation. J. Chem. Phys. **122**, 174508 (2005b)
Neimark, A.V., Vishnyakov, A.: The birth of a bubble: a molecular simulation study. J. Chem. Phys. **122**, 054707 (2005c)
Ohba, T., Kaneko, K.: Internal surface area evaluation of carbon nanotube with GCMC simulation-assisted N2 adsorption. J. Phys. Chem. B **106**, 7171 (2002)
Panagiotopoulos, A.Z.: Adsorption and capillary condensation of fluids in cylindrical pores by Monte Carlo simulation in the Gibbs ensemble. Molec. Phys. **62**, 701 (1987a)
Panagiotopoulos, A.Z.: Direct determination of phase coexistence properties of fluids by Monte Carlo simulation in a new ensemble. Mol. Phys. **61**, 813 (1987b)
Panagiotopoulos, A.Z.: Molecular simulation of phase coexistence—finite-size effects and determination of critical parameters for 2-D and 3-D Lennard–Jones fluids. Int. J. Thermophys. **15**, 1057 (1994)
Panagiotopoulos, A.Z., Quirke, N., Stapleton, M., Tildesley, D.J.: Phase equilibria by simulations in the Gibbs ensemble: alternative derivation, generalization and application to mixtures and membrane equilibria. Mol. Phys. **63**, 527 (1988)
Peterson, B.K., Gubbins, K.E.: Phase transitions in a cylindrical pore—grand canonical Monte-Carlo, mean field-theory and the Kelvin equation. Mol. Phys. **62**, 215 (1987)
Peterson, B.K., Gubbins, K.E., Heffelfinger, G.S., Marini Bettolo Marconi, U., van Swol, F.: Lennard–Jones fluids in cylindrical pores—nonlocal theory and computer simulation. J. Chem. Phys. **88**, 6487 (1988)
Peterson, B.K., Heffelfinger, G.S., Gubbins, K.E., Marini Bettolo Marconi, U., van Swol, F.: Layering transitions in cylindrical pores. J. Chem. Phys. **93**, 679 (1990)
Press, W.H., Flannery, B.P., Teukolsky, S.A., Vetterling, W.T.: Numerical Recipes. Cambridge University Press, Cambridge (1989)
Reid, R.C., Prausnitz, J.M., Poling, B.E.: The Properties of Gases and Liquids. 4th edn. McGraw–Hill, Singapore (1988)
Rowlinson, J.S., Widom, B.: Molecular Theory of Capillarity. Clarendon, Oxford (1982)
Shi, W., Johnson, J.K.: Gas adsorption on heterogeneous single-walled carbon nanotube bundles. Phys. Rev. Lett. **91**, 015504 (2003)
Shi, W., Zhao, X., Johnson, J.K.: Phase transitions of adsorbed fluids computed from multiple-histogram reweighting. Mol. Phys. **100**, 2139 (2002)
Siepmann, J.I., Frenkel, D.: Configurational-bias Monte Carlo—a new sampling scheme for flexible chains. Mol. Phys. **75**, 59 (1992)
Simonyan, V.V., Diep, P., Johnson, J.K.: Molecular simulation of hydrogen adsorption in charged single-walled carbon nanotubes. J. Chem. Phys. **111**, 9778 (1999)
Smit, B., de Smedt, P.H.: Computer simulations in the Gibbs ensemble. Mol. Phys. **68**, 931 (1989)
Talapatra, S., Migone, A.D.: Adsorption of methane on bundles of closed-ended single-wall carbon nanotubes. Phys. Rev. B **65**, 045416 (2002)
Tjatjopoulos, G.J., Feke, D.L., Mann Jr., J.A.: Molecule-micropore interaction potentials. J. Phys. Chem. **92**, 4006 (1988)
Vishnyakov, A., Neimark, A.V.: Studies of liquid–vapor equilibrium, criticality and spinodal transitions in nanopores by the gauge cell Monte Carlo simulation method. J. Phys. Chem. B **105**, 7009 (2001)

Vishnyakov, A., Neimark, A.V.: Nucleation of liquid bridges and bubbles in nanoscale capillaries. J. Chem. Phys. **119**, 9755 (2003a)

Vishnyakov, A., Neimark, A.V.: Monte Carlo simulation test of pore blocking effects. Langmuir **19**, 3240 (2003b)

Vishnyakov, A., Piotrovskaya, E.M., Brodskaya, E.N., Votyakov, E.V., Tovbin, Y.K.: Critical properties of Lennard–Jones fluids in narrow slit-shaped pores. Langmuir **17**, 4451 (2001)

Widom, B.: Some topics in the theory of fluids. J. Chem. Phys. **39**, 2808 (1963)

Williams, K.A., Ecklund, P.C.: Monte Carlo simulations of H2 physisorption in finite-diameter carbon nanotube ropes. Chem. Phys. Lett. **320**, 352 (2000)

Yin, Y.F., Mays, T., McEnaney, B.: Adsorption of nitrogen in carbon nanotube arrays. Langmuir **15**, 8714 (1999)

Yoo, D.H., Rue, G.H., Hwang, Y.H., Kim, H.K.: Study of argon adsorbed on open-ended carbon nanotube bundles. J. Phys. Chem. B **106**, 3371 (2002a)

Yoo, D.H., Rue, G.H., Seo, J.Y., Hwang, Y.H., Chan, M.H.W., Kim, H.K.: Study of nitrogen adsorbed on single-walled carbon nanotube bundles. J. Phys. Chem. B **106**, 9000 (2002b)

Zhang, X.R., Wang, W.C.: Adsorption of linear ethane molecules in single walled carbon nanotube arrays by molecular simulation. Phys. Chem. Chem. Phys. **4**, 3048 (2002)

Zhang, Z., Chakrabarti, A.: Phase separation of binary fluids confined in a cylindrical pore: A molecular dynamics study. Phys. Rev. E **50**, R4290 (1994)